Illumination Correction in Psoriasis Lesion Images

Gabriela Maletti and Bjarne Ersbøll

Department of Informatics and Mathematical Modelling,
Technical University of Denmark,
DK-2800 Kgs. Lyngby, Denmark
{gmm, be}@imm.du.dk
http://www.imm.dtu.dk/image

Abstract. An approach to automatically correct illumination problems in dermatological images is presented. The illumination function is estimated after combining the thematic map indicating skin -produced by an automated classification scheme- with the dermatological image data. The user is only required to specify the class for which its thematic map is most suitable to be used in the illumination correction. Results are shown for real examples. It is also shown that the classification output improves after illumination correction.

1 Introduction

We use a set of 175 *RGB* psoriasis lesion images, of size 556 pixels by 748 pixels, taken at the Gentofte Hospital, Denmark, during pilot sessions with three invited patients. For each patient, three lesions were followed once a week during at least three weeks. In each session, five images of each lesion were taken. Examples can be seen in Figure 3. The skin images are affected by shadows due to the non-plane shape of the objects. Thanks to the use of an integrating sphere [1] (see Figures 1 and 2) with optimal illumination conditions some skin images [6] could be corrected. The sphere assumes that the captured objects are plane. A quadratic model is assumed for the objects, because, for instance, an arm or a leg, as a first approximation, is similar to a cylinder than to a plane.

On the other hand, in an ideal situation, for a given lesion, the classification output should contain a repeated pattern within and between sessions. It could be nice to count with an algorithm that selects automatically, from the thematic maps, the objects to be aligned. However, as it was reported in [4], for many examples without any illumination correction, this is not a possibility. Thus, alignment and registration could turn to be a difficult -if not impossible- task. In order to be able to produce valid results regarding the actual data-set, an illumination correction scheme is proposed here.

This report is organized as follows. The first part is composed by the proposed Illumination Correction Scheme and the general results. The second part

Fig. 1. Integrating sphere with optimal illumination conditions used to capture the images.

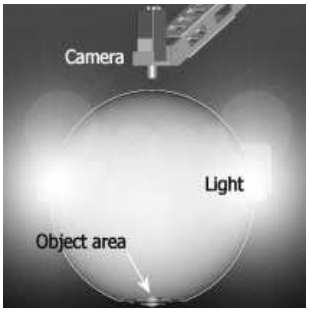

Fig. 2. Sketch of the sphere integrating lighting technology with camera technology. Thanks to Videometer [1] for providing this Figure.

is composed by the Appendix, which contains results for each psoriasis image belonging to the data set. This was done so It is included for the reader interested on analyzing the results in detail.

2 Illumination Correction Scheme

A set of data for which it can be assumed that in each neighborhood the data have the same distribution is required. The images of lesions with psoriasis can be assumed to contain three classes: background, normal skin and lesion. In order to segment the lesions, a two-stage hierarchical classification scheme -originally reported in [4]- has been proposed. The user is required to select the class which he considers most suitable to be used as input to the Illumination Function Estimation scheme. Neighborhoods of pixels belonging to that class are assumed to satisfy the same homogeneity criteria. Data are interpolated and the illumination function is estimated from these data. Details follow.

2.1 Classification Scheme

For completeness, general aspects of the scheme proposed in [4] are given here. Basically, in the first stage, the skin is separated from the background, and, in the second stage, the lesion is separated from the normal skin. In both stages, the classes are assumed to be Gaussian distributed. In each stage, means, standard deviations and prior probabilities of the classes were estimated with an Expectation-Maximization Algorithm [7]. These statistics were introduced in a discrimination function [2], which was applied to the output of the convolution of the image with a circular window of optimal size [5].

2.2 Illumination Function Estimation

Following [3], let $i(x, y)$ be the illumination function affecting the original scene $f(x, y)$:

$$g(x, y) = i(x, y)f(x, y) \tag{1}$$

such that $g(x, y)$ is the illumination affected scene. This model assumes that the output is the product between the amount of arriving light and the original scene reflectivity. A first approximation is to assume that

$$i(x, y) = \frac{g_k(x, y)}{\beta_k} \tag{2}$$

where β_k is a constant known after detector calibration.

Let G, F and I be specific images of $g(x, y)$, $i(x, y)$ and $f(r, c)$ respectively. Let $\mathsf{F} = \{f[r, c]\}$ and $\mathsf{G} = \{g[r, c]\}$ be hierarchically defined in terms of $\mathsf{Z} = \{z[r, c]\}$ that represents the partition of the scene in different classes. Each $z[r, c]$ is a value in $\Omega = \{1, \ldots, K\}$, where $z[r, c] = k$ means that the coordinate $[r, c]$ of a pixel belongs to the $k - th$ class. Let $\mu = \{\mu_1, \ldots, \mu_K\}$ be the class means, and $\mathsf{M} = \{m[r, c] = \mu_k / z[r, c] = k \forall k \in \Omega\}$ be such that $m[r, c]$ is the mean of the class the pixel at location $[r, c]$ belongs to. Let N be defined with the local means of G such that $E[\mathsf{N}] = \mathsf{M}$. Let $\hat{\mathsf{N}}_k$ be the interpolation function of sampled values of $\mathsf{N}_k =< \mathsf{N}, \mathsf{Z} = k >$ greater than zero [1]. Then $\hat{I}[r, c] = \frac{\hat{\mathsf{N}}_k[r,c]}{O_k}$ and O_k is the normalization factor.

Body parts are modelled with a quadratic function. The interpolation function is given by:

$$\boldsymbol{y}_{Px1} = \left[\boldsymbol{\theta}_{Px1}\ \mathbf{1}_{Px1}\ \boldsymbol{r}\ \boldsymbol{c}\ \boldsymbol{rr}\ \boldsymbol{cc}\right] \tag{4}$$

[1]

$$< \mathsf{N}, \mathsf{Z} = k > \tag{3}$$

is the scalar product between the tensor N and the thematic map that has, in a given location the value one, if the corresponding pixel belongs to the k-th class and the value zero otherwise.

where y_i is the local mean value $n_k[r_i, c_i]$ for a given band and $[r_i, c_i]$ is the location of the i-th pixel sampled, which belongs to the k-th class. $\boldsymbol{r} = [r_1, \ldots, r_P]^T$, $\boldsymbol{c} = [c_1, \ldots, c_P]^T$ and $\boldsymbol{rc} = [r_1 c_1, \ldots, r_P c_P]^T$, $\boldsymbol{rr} = [r_1 r_1, \ldots, r_P r_P]^T$ and $\boldsymbol{cc} = [c_1 c_1, \ldots, c_P c_P]^T$. The normalization factor O_k is the maximal value of $(\hat{G}_k[r, c] + \gamma)$ and γ is the minimal constant added to $G_k[r, c]$ such that the output is positive.

This procedure can be applied to each single image band. Thus, for multispectral images, the output of the present scheme is a multi-spectrally estimated illumination function.

3 Results and Discussion

The algorithm that estimates the illumination function requires that, for each single image, a map of an expected homogeneous region must be provided. On the other hand, the problem is precisely that the classification can not be done in a uniform way and for this reason, the illumination correction is needed. As was mentioned before, it is assumed that the images of lesions with psoriasis contain three classes: curtain, normal skin and lesion. The best candidate to be interpolated is the normal skin, because it usually appears in different parts of the image. However, there are cases for which we could consider that the whole image is pure lesion. For this reason, each set of images corresponding to the same lesion was treated separately. For the images of the first patient, it was possible to provide a rough estimation of the maps corresponding to the normal skin. These maps were the output of the second stage of the classification scheme used. However, for the remaining cases, the maps of the skin, including lesions[2], were used to estimate the illumination function. The thematic maps produced in the classification scheme combined with the original images used as input for the illumination correction stage are shown in Figure 3. As it can be seen, for the cases $1A$, $1B$ and $1C$, the region mapping normal skin was used. For the cases $2A$ and $3A$, a map indicating the whole image was generated. For the cases $2B$, $2C$, $3B$ and $3C$ the thematic map indicating skin was selected.

The image region to be modelled was convolved with a circular window with a diameter of eleven pixels, empirically found. In order to reduce, during the convolution, the influence of pixel values belonging to other classes in the region borders, pixel values to be excluded from the model were previously replaced with the mean value of the data to be modelled. This was also done in order to preserve the correct shadow information of the region to be modelled. An artificial grid was placed on the whole image, and grid pixels belonging to the region to be modelled were sampled.

[2] This means the output of the first stage of the classification scheme

The estimated multi-spectral illumination functions and the corresponding estimated illumination-corrected images can be seen in Figure 4. The estimated illumination function for each single image of the psoriasis image set can be found in Appendix A. Note that the extrapolation errors mostly occur in the background, which really does not contain information of interest anyhow.

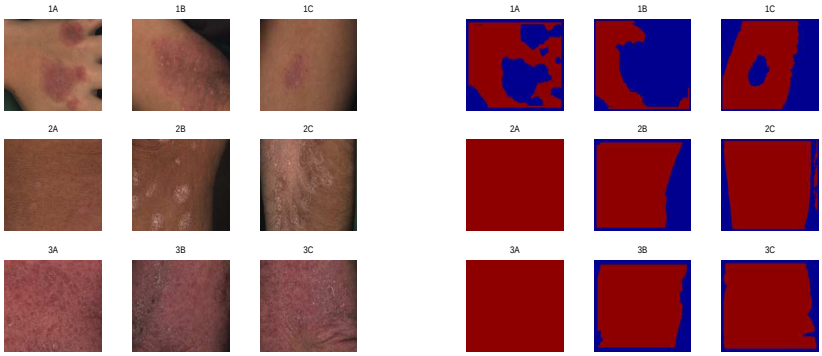

Fig. 3. Examples of original images of lesions with psoriasis (left) and the thematic maps (right) outputs of the classification scheme used in the illumination function estimation.

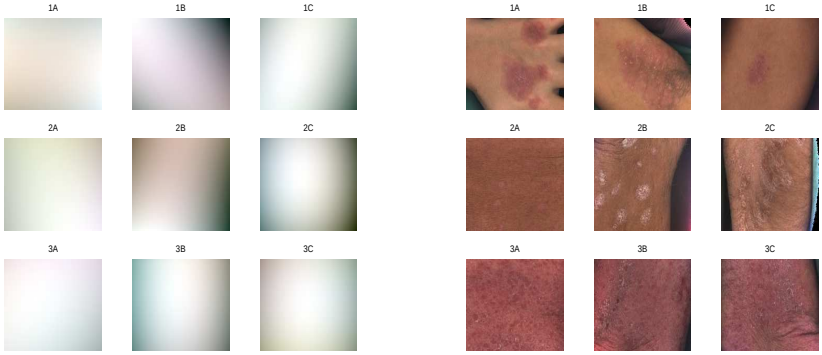

Fig. 4. Estimated illumination functions of the images of Figure 3 (left) and the corresponding illumination corrected images (right).

Comments based on visual assessment of the illumination functions of each group of images of the same lesion follow. It is quite obvious that a quadratic model is not very representative of an object like a hand. This is reflected in the illumination function, which does not include the shadows between the fingers. Continuing with the next lesion, we can observe that part of the lesion B of patient 1 is covered by shadow in the original images. In spite of the illumination function being almost the same for all the captures, it has to be noted, that the lesion presents occlusions in some cases, which means that, along the captures, the shadow is not affecting a given part of the lesion in the same way. With respect to lesion C of patient 1, which is placed in the center of the image, it seems that the illumination correction would not improve future alignment and registration outputs very much. However, note in the illumination corrected images, that the shadows are not removed. Note in [4] that the provided thematic maps indicating skin do not include the regions covered by shadows. Results could be improved finding better the cost values for the discrimination function in the classification scheme. For the lesion A of patient 2 it is noted that the illumination model represents the shadows that appear on the left of the images in the second and fourth session quite well. Comparing the classification output after illumination correction with the classification output using the original data (see [4]), it can be deduced, that, for this case, the illumination correction is clearly necessary. Looking at the illumination corrected images of patient 2, lesion B it can be noted that the illumination model does not correct the shadows in some captures well. This is due to the fact that the thematic map of the skin does not include parts of the shadows, which were assigned to the class curtain in the first classification stage: changes in the cost values could improve the results obtained. For the case $(2, C)$, it is noted that the classification output improves when the illumination is corrected. In spite of being extrapolation errors in the curtain, they obviously do not affect the classification between normal skin and lesion. The illumination functions of the case $(3, A)$ seem to represent the shadows on the original images well. This case is quite difficult, because it is hard to identify correspondent points in the images by visual assessment. Therefore, to evaluate the classification output is difficult. However, for same pairs of sessions, some kind of repeated structure can be observed. The classification output within sessions after illumination correction of the images of the case $(3, B)$ does not look very convincing. This may be due to the spherical shape of the illumination function, which is not representative of the body part modelled. Note in the illumination corrected images the light areas on the image corners. A better thematic map of the region to be modelled could improve the results obtained. For the case $(3, C)$, skin displacements attained after folding the elbow allow to identify corresponding points visually. By comparing the classification outputs after illumination correction within sessions, in general, they contain a repeated pattern. However, for some pairs of sessions, particularly the last ones, is not quite obvious how the correspondence should be.

The normalized histograms of the region indicating skin was again calculated for each single |B-G| band. Table 1, comparable to Table 2 in [4], was constructed. [3]. Details can be found in Table 2. As it can be observed, in general, the correlation values are smaller than before. The large correlation values before illumination correction could be due to the illumination itself and the actual correlation values are more real for the skin data. It is suggested to extrapolate statistics from one single image to another only after normalization.

Table 1. Average and standard deviation correlation value between the histogram of a normalized illumination-corrected image band and the normalized histogram of the normalized bands of the illumination-corrected images belonging to the same session.

(Patient, Lesion)	μ_a	σ_a	μ_b	σ_b	μ_c	σ_c	μ_d	σ_d
(1,A)	0.6031	0.1133	0.5716	0.0760	0.5757	0.1365	0.5989	0.1250
(1,B)	0.5354	0.1547	0.3669	0.1081	0.3671	0.0933	0.3551	0.0745
(1,C)	0.6550	0.1090	0.6850	0.0869	0.7539	0.1096		
(2,A)	0.6149	0.1154	0.7712	0.0542	0.4616	0.0846	0.4831	0.1299
(2,B)	0.4000	0.0547	0.5591	0.1029	0.4901	0.0693	0.3961	0.0262
(2,C)	0.3421	0.0441	0.4627	0.1523	0.5447	0.0915	0.4285	0.0573
(3,A)	0.5196	0.0717	0.6408	0.1374	0.3968	0.0896	0.4179	0.0456
(3,B)	0.5913	0.0636	0.4585	0.0818	0.3425	0.0239	0.3450	0.0821
(3,C)	0.4813	0.1172	0.4678	0.0337	0.5518	0.0994	0.4702	0.0626

The same thematic maps indicating skin generated in the previous classification using the original images, were assumed to be the output of the first classification stage using the images with illumination correction. The outputs of the second stage of the classification scheme are shown in Subsection C. In order to avoid extrapolation errors, the discrimination function was computed for each single image separately.

As it can be seen, thematic maps of some lesions, have some repeated patterns in common. Based on this, it is considered that the output of the illumination correction is a better estimation of the expected data. However, in order to be able to automatically select corresponding objects in the thematic maps of the same lesion, further work needs to be done. Since it is not the main objective of the present work, the cases for which it was not possible to automatically define corresponding objects, manually selection after visual inspection of the images is suggested.

It should to be mentioned that in many cases, shadows in the skin were assigned to the class curtain. This did not allow the introduction of the correct slope of the surface that represents the skin in the illumination model. Finding

[3] For computational details, see Equations 4 and 5 in [4]

better cost values to use use in the discrimination functions is encouraged in order to improve the obtained results.

4 Conclusions

A new scheme for illumination correction in dermatological data that combines conventional tools has been proposed. The classification scheme used has been shown to produce suitable thematic maps to be used in the estimation of the illumination function affecting the scene. It has also been shown that the illumination corrected images are a better input for the second stage of the classification scheme. After illumination correction, the classification results improved in cases for which it was not possible to produce thematic maps with a repeated pattern previously. By visual assessment of the results, it is encouraging to extend the scheme to other application areas.

Acknowledgments

To the SITE Project funded by a grant from the Danish Technical Research Foundation (Project Number *STVF* 56-00-0123) for supporting the present work. To the dermatologists Lone Skov and Bo Bang of the Gentofte Hospital of Denmark and to the anonymous patients, for their collaboration during the image acquisition sessions.

Appendix

A Illumination functions

Fig. 5. Illumination functions of the original images of (Patient 1, Lesion A).

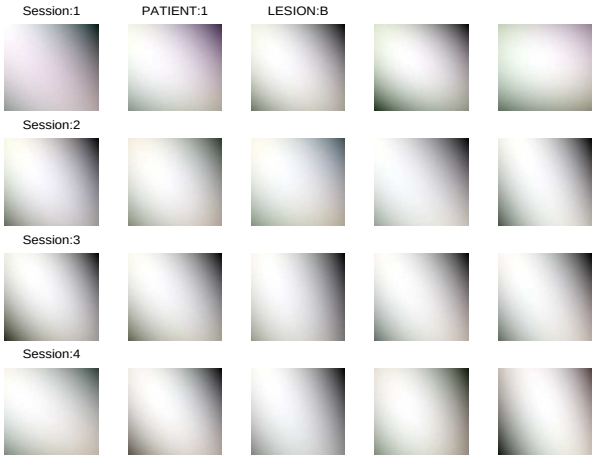

Fig. 6. Illumination functions of the original images of (Patient 1, Lesion B).

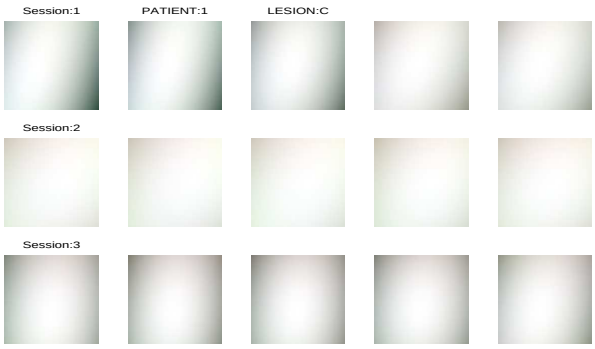

Fig. 7. Illumination functions of the original images of (Patient 1, Lesion C).

Fig. 8. Illumination functions of the original images of (Patient 2, Lesion A).

Fig. 9. Illumination functions of the original images of (Patient 2, Lesion B).

Fig. 10. Illumination functions of the original images of (Patient 2, Lesion C).

Fig. 11. Illumination functions of the original images of (Patient 3, Lesion A).

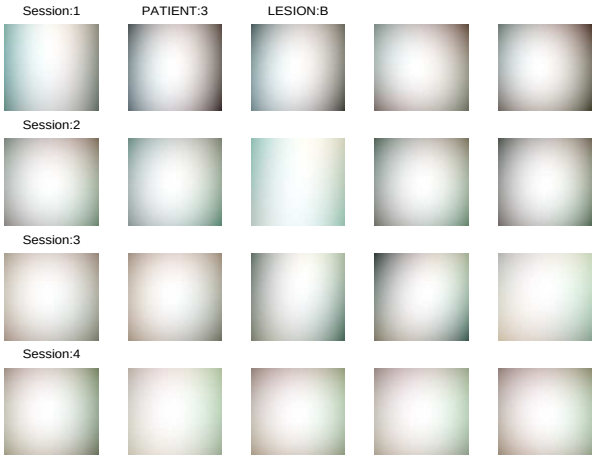

Fig. 12. Illumination functions of the original images of (Patient 3, Lesion B).

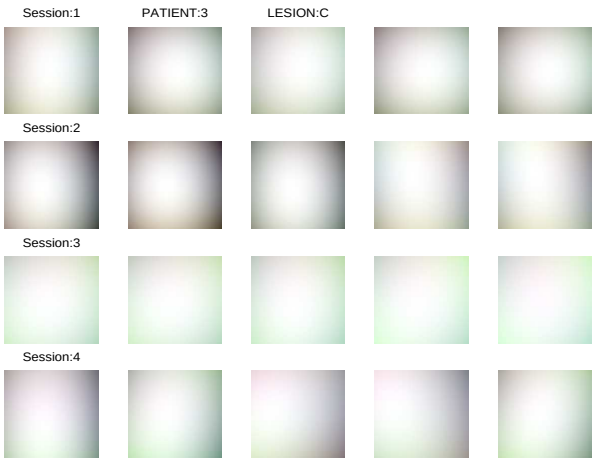

Fig. 13. Illumination functions of the original images of (Patient 3, Lesion C).

B Illumination corrected images

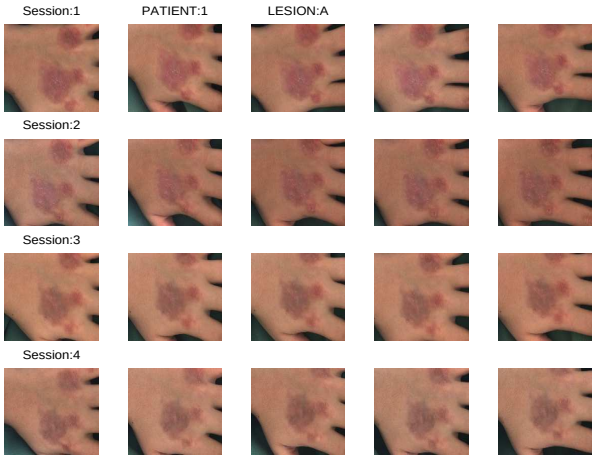

Fig. 14. Images of (Patient 1, Lesion A) after illumination correction.

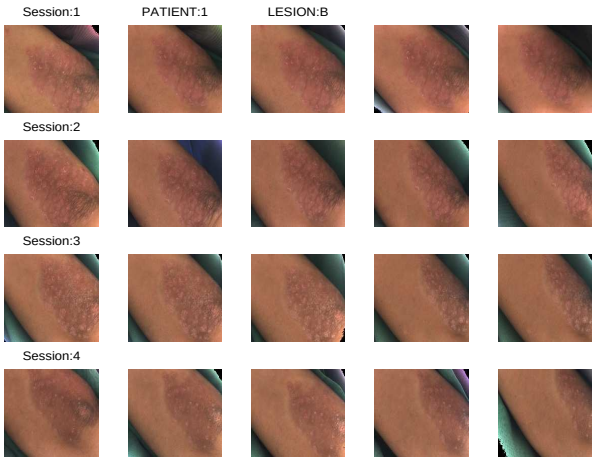

Fig. 15. Images of (Patient 1, Lesion B) after illumination correction.

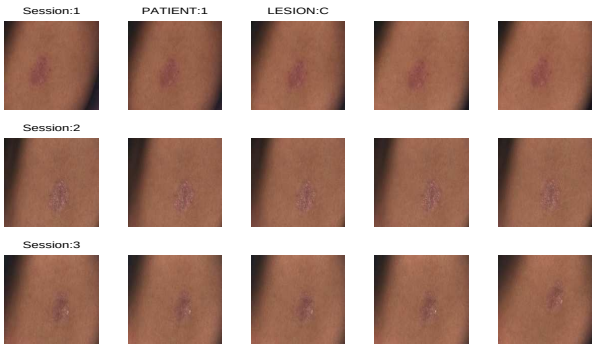

Fig. 16. Images of (Patient 1, Lesion C) after illumination correction.

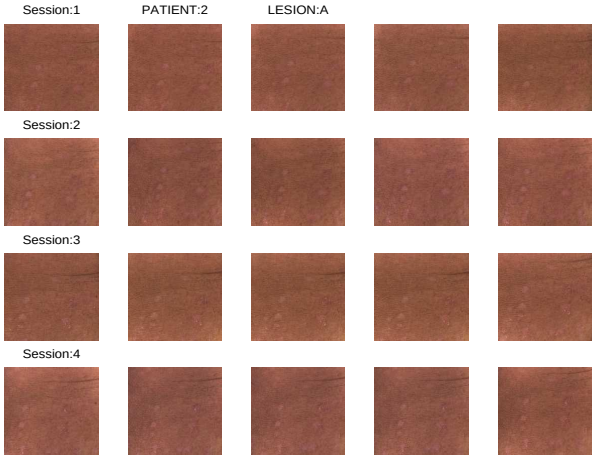

Fig. 17. Images of (Patient 2, Lesion A) after illumination correction.

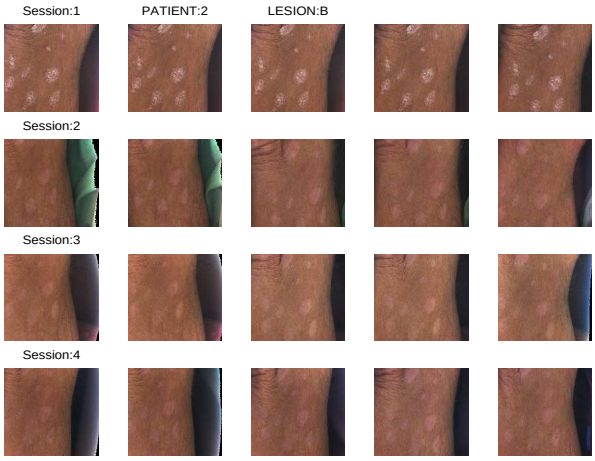

Fig. 18. Images of (Patient 2, Lesion B) after illumination correction.

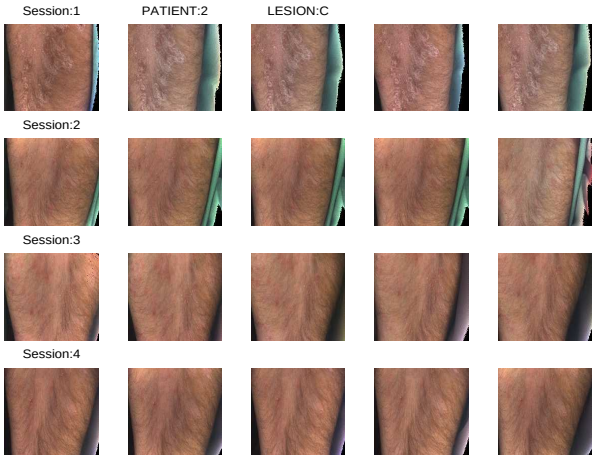

Fig. 19. Images of (Patient 2, Lesion C) after illumination correction.

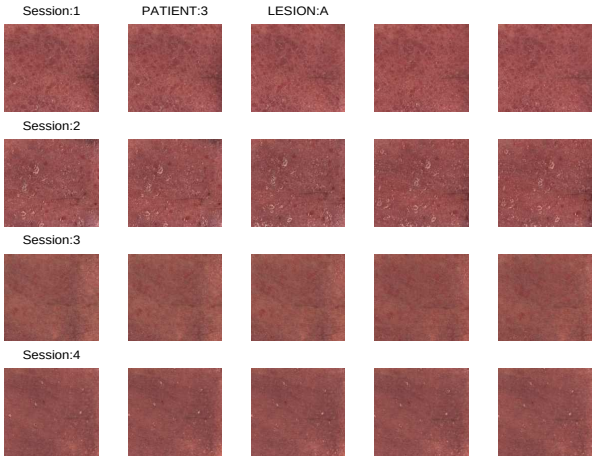

Fig. 20. Images of (Patient 3, Lesion A) after illumination correction.

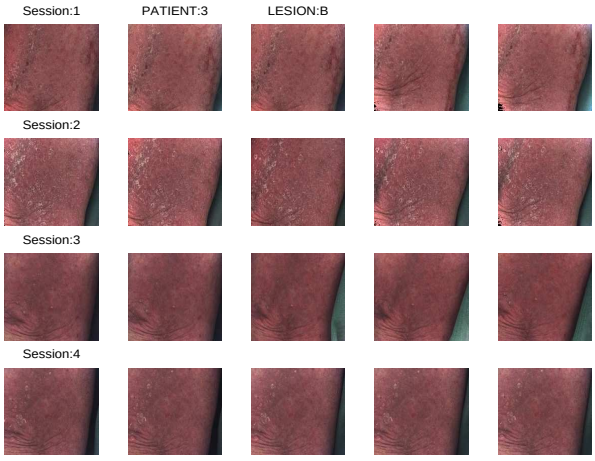

Fig. 21. Images of (Patient 3, Lesion B) after illumination correction.

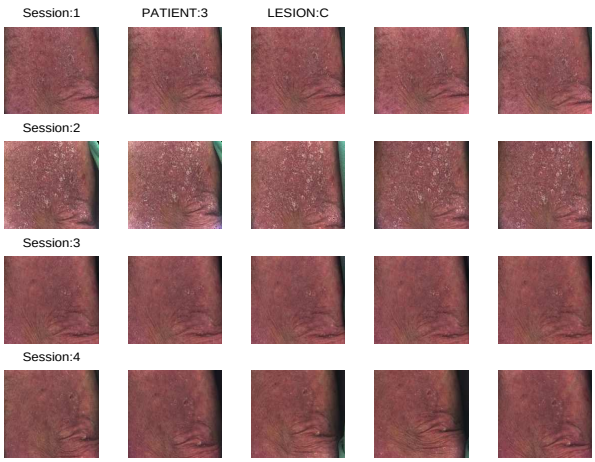

Fig. 22. Images of (Patient 3, Lesion C) after illumination correction.

Table 2. Average correlation values of the normalized histogram of the |B-G| band skin data of each single corrected image with the normalized histogram of the |B-G| band skin data of the corrected images that belong to the same session than that.

Capture	$(1,A)$	$(1,B)$	$(1,C)$	$(2,A)$	$(2,B)$	$(2,C)$	$(3,A)$	$(3,B)$	$(3,C)$
a1	0.6155	0.3172	0.7399	0.7006	0.4071	0.3594	0.5819	0.6593	0.5928
a2	0.6107	0.6505	0.7344	0.6982	0.4515	0.2797	0.4596	0.5422	0.4386
a3	0.6944	0.4272	0.7096	0.6887	0.4162	0.3514	0.4640	0.6583	0.6006
a4	0.4121	0.6614	0.6049	0.5386	0.3069	0.3222	0.6117	0.5698	0.4538
a5	0.6828	0.6205	0.4861	0.4483	0.4184	0.3978	0.4810	0.5267	0.3208
b1	0.5682	0.1986	0.7548	0.7964	0.6628	0.3162	0.7402	0.4282	0.4367
b2	0.4687	0.4596	0.6169	0.8109	0.6593	0.5622	0.7367	0.3680	0.4961
b3	0.6497	0.4624	0.7436	0.7443	0.4637	0.6063	0.4906	0.5456	0.5097
b4	0.5311	0.3413	0.7426	0.6886	0.4475	0.5486	0.4900	0.5441	0.4369
b5	0.6405	0.3727	0.5669	0.8157	0.5621	0.2799	0.7464	0.4065	0.4595
c1	0.3731	0.2717	0.8276	0.3583	0.5686	0.4148	0.3528	0.3160	0.5978
c2	0.6779	0.3465	0.6987	0.4786	0.3974	0.6229	0.4282	0.3344	0.5948
c3	0.4952	0.2880	0.5855	0.5422	0.4491	0.4847	0.4726	0.3351	0.5897
c4	0.6554	0.4677	0.8287	0.5392	0.5425	0.6186	0.2616	0.3461	0.6024
c5	0.6768	0.4615	0.8288	0.3900	0.4931	0.5826	0.4685	0.3807	0.3742
d1	0.6438	0.3840		0.3499	0.3912	0.4589	0.3807	0.4331	0.4318
d2	0.6685	0.3044		0.3363	0.4080	0.4788	0.4702	0.3092	0.5418
d3	0.6429	0.2590		0.5912	0.3533	0.4002	0.4609	0.2485	0.4083
d4	0.6630	0.3779		0.5395	0.4066	0.4633	0.4072	0.3055	0.5336
d5	0.3763	0.4502		0.5988	0.4214	0.3410	0.3706	0.4289	0.4355

C Image classification after illumination correction

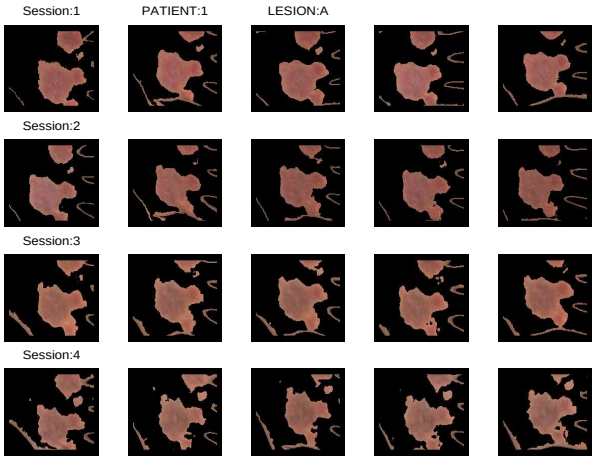

Fig. 23. Overlay of the thematic maps with the images for (Patient 1, Lesion A) after illumination correction.

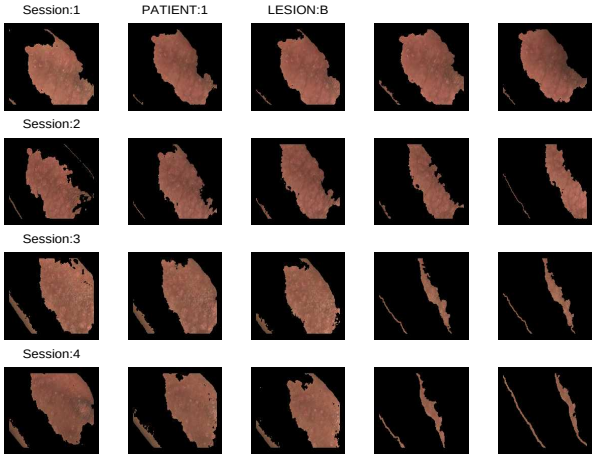

Fig. 24. Overlay of the thematic maps with the images for (Patient 1, Lesion B) after illumination correction.

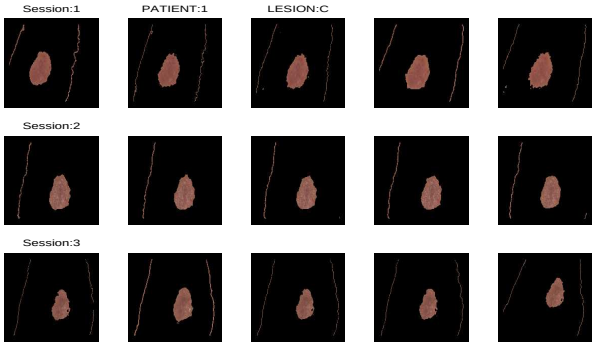

Fig. 25. Overlay of the thematic maps with the images for (Patient 1, Lesion C) after illumination correction.

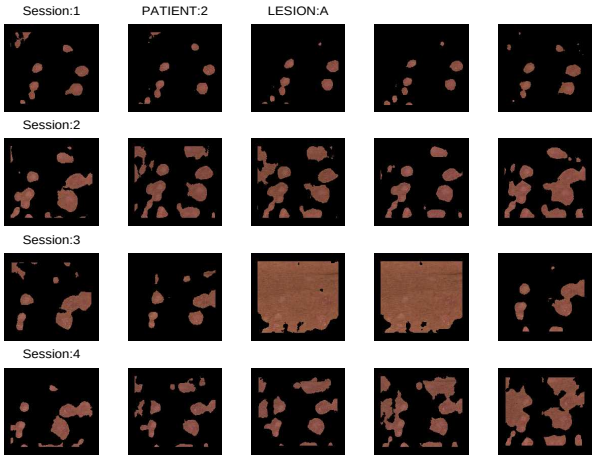

Fig. 26. Overlay of the thematic maps with the images for (Patient 2, Lesion A) after illumination correction.

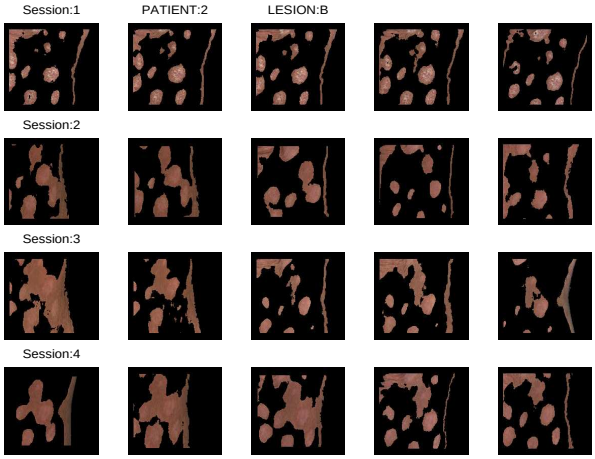

Fig. 27. Overlay of the thematic maps with the images for (Patient 2, Lesion B) after illumination correction.

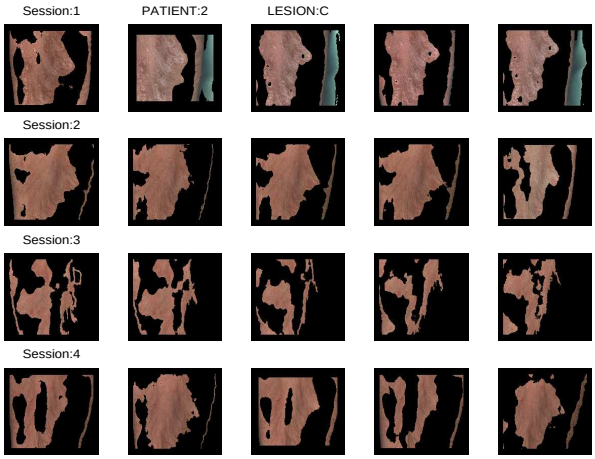

Fig. 28. Overlay of the thematic maps with the images for (Patient 2, Lesion C) after illumination correction.

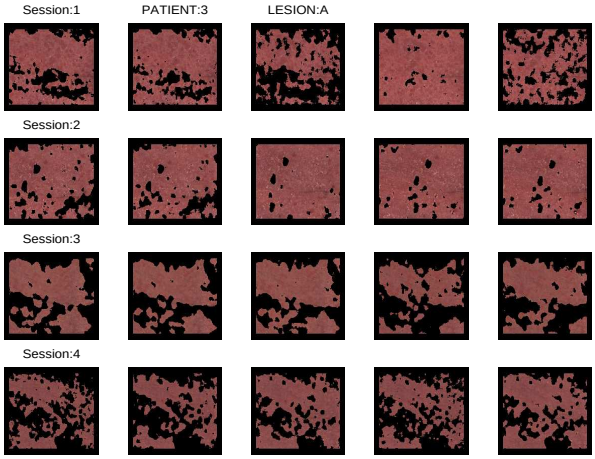

Fig. 29. Overlay of the thematic maps with the images for (Patient 3, Lesion A) after illumination correction.

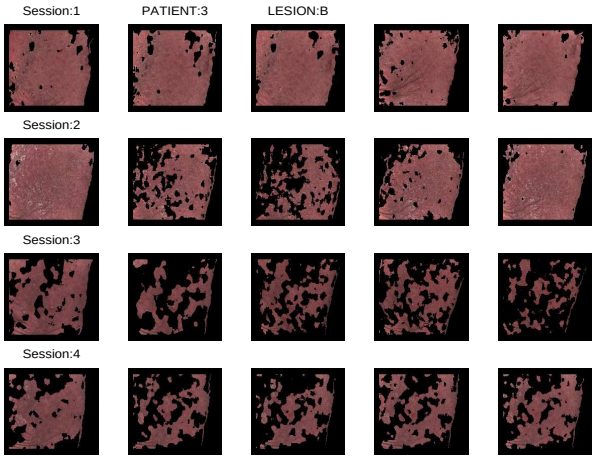

Fig. 30. Overlay of the thematic maps with the images for (Patient 3, Lesion B) after illumination correction.

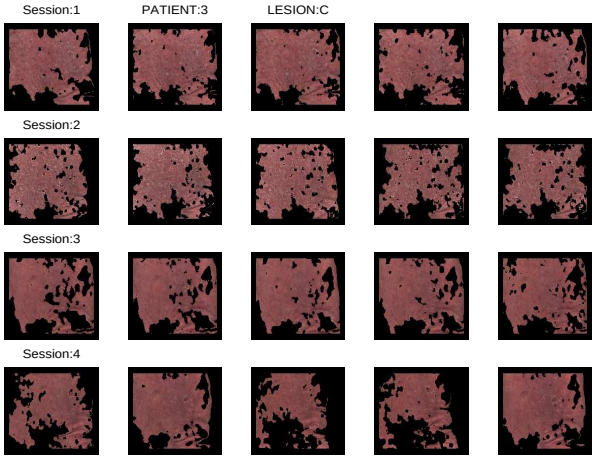

Fig. 31. Overlay of the thematic maps with the images for (Patient 3, Lesion C) after illumination correction.

References

1. Videometer. http://www.videometer.dk.
2. K. Conradsen. *En Introduktion til Statistik. Bind 2.* IMSOR DTH., Lyngby, 1984.
3. J. Lira. *Introducción al Tratamiento Digital de Imágenes.* Instituto Politécnico Nacional, Universidad Nacional Autónoma de México, Fondo de Cultura Económica., México D.F., 1 edition, September 2002.
4. G. Maletti and B. Ersbøll. A hierarchical classification scheme of psoriasis images. Technical Report 6, Department of Informatics and Mathematical Modelling. Technical University of Denmark., Kgs. Lyngby. Denmark., March 2003.
5. G. Maletti, B. Ersbøll, and K. Conradsen. A contextual classifier that only requires one prototype pixel for each class. *IEEE Transactions on Nuclear Science*, 49(3):700–706, June 2002.
6. U. Mattsson, A Jönsson, M. Jontell, and J. Cassuto. Digital image analysis (dia) of color changes in human skin exposed to standardized thermal injury and comparison with laser doppler measurements. *Computer Methods and Programs in Biomedicine*, 50:31–42, 1996.
7. Y. Wang and T. Adali. *Signal Processing for Magnetic Resonance Imaging and Spectroscopy. Stocastic Model Based Image Analysis*, chapter 14, pages 1–34. 2000. (Topics in Biomedical Imaging Course Notes.).